RESEARCH ARTICLE

Comparative evaluation of vat photopolymerization and steel tool molds on the performance of injection molded and overmolded tensile specimens

Xun Jian[1] | Ke Gong[2,3] | Vicente Moritz[3] | Alexandre Portela[3] |
Yinshi Lu[3] | Wenyi Du[3] | Ian Major[3]

[1]Jiangxi Water Resources Institute, Nanchang, Jiangxi Province, China

[2]Bernal Institute, University of Limerick, Limerick, Ireland

[3]PRISM Research Institute, Technological University of Shannon, Athlone, Ireland

Correspondence
Ke Gong, Bernal Institute, University of Limerick, Limerick V94 T9PX, Ireland.
Email: ke.gong@tus.ie

Ian Major, PRISM Research Institute, Technological University of Shannon, Athlone N37 HD68, Ireland.
Email: ian.major@tus.ie

Abstract

This study explores the use of vat polymerization stereolithography (SLA) for fabricating mold tooling, subsequently utilized in injection molding (IM) and overmolding of tensile specimens and directly compared to those produced using metal molds. The results first find the manufacturing time for an SLA-fabricated mold is remarkably short, approximately 6 h, presenting a substantial improvement over traditional methods. Mechanical testing revealed that the tensile specimens from the SLA-fabricated molds exhibited the highest tensile strength among all overmolding batches. This performance was consistent with the tensile bars produced using metal molds, demonstrating the viability of SLA-fabricated molds for overmolding applications and highlighting the potential of FDM to customize the properties of final products. However, variations in mold types impacted the dimensional tolerance and tensile strength of the final specimens. Metal mold-fabricated tensile bars exhibited superior dimensional accuracy and maximum tensile strength (50.6–61.7 MPa) compared to those produced with SLA-fabricated molds (46.9–55.9 MPa). These differences are attributed to the rougher surface finish inherent to the layer-by-layer construction of SLA and the internal stresses and defects resulting from lower thermal conductivity and uneven cooling. In conclusion, this study underscores the promising future applications of SLA-fabricated molds in overmolding, offering reduced manufacturing costs and enhanced design freedom. The findings support the potential of SLA to revolutionize mold fabrication, thereby extending its utility and optimizing the production of polymer components with customized properties.

Highlights
- SLA molds compared to metal molds for direct injection molding and overmolding.
- FFF preforms with varied geometries were overmolded to finalize the specimens.

- Joint configurations in overmolding improved tensile performance.
- Overmolding showed better dimensional accuracy than FFF specimens.
- SLA mold preparation significantly reduced manufacturing costs.

KEYWORDS

joint configuration, manufacturing cost, overmolding, stereolithography (SLA), thermal conductivity

1 | INTRODUCTION

Overmolding is an advanced manufacturing technique that enables the creation of a unified substrate with varied properties by molding one material onto inserted preforms.[1–3] This process is crucial for ensuring the safe bonding of components throughout their service life.[4] Overmolding has been extensively employed in diverse fields such as automotive[5,6] and medical devices.[7] Initially, overmolded articles were produced by molding polymer onto injection-molded preforms,[8,9] which limited the performance and functionality of the final products. This limitation has led to the exploration of alternative methods for preform fabrication, notably additive manufacturing (AM).[10,11] In this context, preforms fabricated using AM can impart tailored characteristics to the finalized articles, with the overmolded polymer providing additional features and enhanced quality.[12]

AM, also known as 3D printing, has been popularized in several fields, including research,[13] medicine,[14] aerospace,[15] dental,[16] and food.[17] It encompasses several techniques,[18] including material extrusion,[19] material jetting,[20] vat photopolymerization,[21] binder jetting,[22] powder bed fusion,[23] sheet lamination,[24] and direct energy deposition.[25] Among these, fused filament fabrication (FFF) and stereolithography (SLA) are the most commonly used by practitioner.[26–28] FFF, pioneered by Stratasys Corporation under the RepRap project.[29] It involves feeding material through a heated area and forcing it through a nozzle to be deposited onto a building platform in the desired geometries.[30] The nozzle moves in the X–Y plane first and then layer-by-layer (stacking in the z-axis) until the object is fully fabricated.[31] This technique has been widely employed due to its ease of use,[32] versatility in material usage,[33] and rapid prototyping efficiency. However, FFF-fabricated specimens still face challenges in surface quality and dimensional precision, which are critical in applications demanding high accuracy.[34]

To date, several studies have overmolded FFF-fabricated preforms to finalize the components. Fuenmayor et al.[35] applied this route in the pharmaceutical field, finding that finalized tablets could be efficiently manufactured with tailored characteristics. The mechanical performance of these components was investigated by Gong et al.[2,12,36] focusing on the employed materials and joint configurations. These studies revealed that varied materials in preform and overmolding techniques could result in poor mechanical performance, which could be mitigated by appropriate joint configurations in the final components. Rajamani et al.[37] demonstrated that increasing the contact surface and adding carbon fiber to preforms improved bonding strength between FFF preforms and overmolded ribs. Smith et al.[38] overmolded ultra-high-molecular-weight polyethylene onto PEEK preforms for orthopedic implant applications, achieving promising characteristics with a honeycomb topology and 60% infill density. This result indicates that polymer–polymer overmolding could potentially replace high-demand metals in orthopedic implants. Nevertheless, the high cost and extended fabrication time for newly designed molds remain significant barriers.

SLA is a vat photopolymerization AM technique that fabricates articles layer-by-layer using a UV laser to cure liquid resin into solid parts.[39] SLA can be employed to produce molds with desired characteristics due to its high resolution and low manufacturing cost. Moritz et al.[40] obtained several polypropylene tensile bars using SLA-fabricated molds and found that different SLA materials could affect tensile performance due to varying cooling conditions. Basile et al.[41] created some SLA-fabricated molds with micro-textured surfaces to produce medical components, tailoring the microstructures of finalized products efficiently and cost-effectively. Keane et al.[42] demonstrated the promising impact of abrasive blasting and sanding in reducing surface roughness with minimal geometric loss.

In this study, various FFF-fabricated inserts with different geometries were overmolded using SLA-fabricated and metal molds to assess their tensile performance. This approach aims to leverage future overmolding techniques for enhanced personalization of final products. Integrating FFF-fabricated inserts with overmolding in SLA-designed molds represents a significant advancement in manufacturing technology. This method not only addresses the limitations of using FFF or SLA independently but also enables the production of complex, high-quality parts tailored to specific application requirements. Industries such as automotive, aerospace, consumer electronics, and medical

devices are increasingly adopting this hybrid manufacturing technique to achieve more efficient, cost-effective, and innovative production solutions.

2 | METHODOLOGY

2.1 | Material

The polyethylene terephthalate glycol (PETG) filament in the diameter of 1.75 mm was purchased from Real Filament Company in Netherlands. It was first dried at 40°C for 8 h and then carried into FFF process. In case of the IM processing, the PETG pellets were obtained by pelletizing the purchased PETG filament. The material employed in the SLA process was FormLabs Rigid 10 K resin, obtained from FormLabs Ltd.

2.2 | SLA-fabrication of mold tooling

The SLA-fabricated mold with the same dimension of metal mold, which was designed using SolidWorks 2023 Edition Software (Dassault Systèmes, Waltham, USA), was shown in Figure 1A. The designed mold consists of runners, gates, and two cavities of tensile specimen. The mold was fabricated using a FormLabs 2 (FormLabs Ltd.) SLA 3D printer as shown in Figure 1B based on the parameters of 250 mW laser at 405 nm wavelength, layer thickness of 50 μm in a 45° orientation with respect to the top plane.

2.3 | Tensile specimen fabrication

Three groups of specimens were fabricated under five duplicates each batch via the following three routes: FFF only, IM only, and overmolding, where the SLA-fabricated and metal molds were used in both IM and overmolding processes. The overmolded batches were manufactured in two steps: FFF fabricated the preforms with three geometries and these preforms were overmolded. The finalized dimension is according to ASTM-D638-3 with nominal values presenting in Figure 2.

In case of the FFF-fabricated specimens and preforms for overmolding stage, designs were created using SolidWorks 2023 Edition Software and exported as STL files, which were then sliced using Creality Print Software. The tensile bars were manufactured with an Ender-3V3 KE 3D Printer (Creality, Shenzhen, China) using a 0.4-mm diameter nozzle based on the z-axis shown in Figure 2. FFF process parameters were: layer thickness (0.1 mm), top/bottom solid layers (1), outline/perimeter
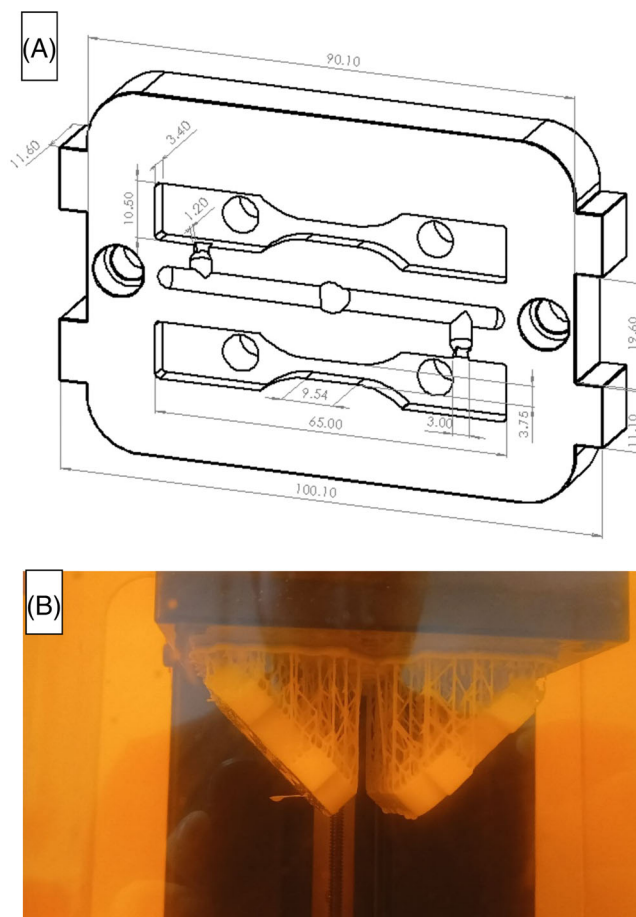

FIGURE 1 SLA-fabricated mold in (A) schematic graph and (B) SLA-fabricated molds.
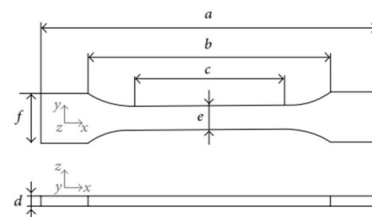
Tensile Bar	Dimension (mm)					
	a	b	c	d	e	f
Measurement	64	30	12.7	3.2	3.3	10

FIGURE 2 Tensile bar dimensions.

shells (2), raster angle (±45°), building platform temperature (80°C), extrusion temperature (240°C), infill density (100%), and printing speed (100 mm/s).

The IM tensile bars were produced using a Babyplast 6/12 injection molding machine (Rambaldi Corporation, Molteno, Italy) with the parameters shown in Table 1.

TABLE 1 Employed parameters in injection molding process.

Injection pressure parameter	Value	Unit
Plasticizing temperature	220	°C
Chamber temperature	210	°C
Nozzle temperature	190	°C
Shot size	45	mm
Cooling time	30	s
Injection pressure	70	bar
Injection pressure time	5	s
Holding pressure	60	bar
Holding pressure time	5	s
Holding pressure setting	4	mm
Decompression	4	mm
Injection speed	95	%
Holding speed	50	%
Mold temperature	40	°C

For overmolded specimens, fabrication included two stages: (a) creating FFF inserts with varied geometries, and (b) inserting the FFF-fabricated inserts into mold cavities and performing the overmolding process. The parameters for insert fabrication were identical to those for FFF-fabricated tensile bars. The geometries of FFF-fabricated inserts are based on our previous finding that the half-thickness series specimens show a comparable tensile behavior compared to the IM tensile bar.[43] It can be seen in Figure 3 that the half-thickness preform owns a 1.6 mm height and it can be stacked or removed a $64 \times 1 \times 1$ (mm) cuboid to create the another two preforms. Overmolding stage parameters matched those used for IM-fabricated specimens, with the shot size adjusted to 28 mm.

2.4 | Dimension observation

All fabricated specimens were examined using a Nikon ShuttlePix P-MFSC Digital Microscope to determine their dimensions (tolerance), with five replicates in each batch. Three main parameters (thickness, total length, and width) were measured and compared to the ideal dimensions.

2.5 | Tensile analysis

Tensile tests were conducted to evaluate the effect of different manufacturing processes on tensile strength and modulus, following ASTM-D638-3 standards. Tests were performed using an LRX single-column, bench-mounted

material testing system (JLW Instruments Corporation, UK) with a 5 kN load cell, at a crosshead speed of 5 cm/min at room temperature. Maximum tensile strength (σ), Young's modulus (E), and tensile strain (ϵ) were measured.

The formulae utilized in tensile test can be found from Equations (1)–(3), in which P is the testing load, A is the cross-section area, ΔL is the displacement of the crosshead, and L is the gauge length. These results were all calculated and then exported from the NEXYGEN™ software.

$$\sigma = P/A \tag{1}$$

$$E = \sigma/\epsilon \tag{2}$$

$$\epsilon = \Delta L/L \tag{3}$$

2.6 | Fracture observation

Fractured sections were analyzed using a Mira Scanning Electron Microscope (SEM) from Tescan Oxford Instruments, United Kingdom, operating at 10 kV and 70× magnification. Sections were cut from the fractured tensile bars, gold-coated with an Agar Sputter Coater (Agar Scientific, United Kingdom), and then observed under SEM.

2.7 | Statistical analysis

Experimental data from the tensile tests were analyzed using Minitab 21.0 Software (Minitab Inc., PA, USA) employing the analysis of variance (ANOVA) method. In this case, the varied joint configuration and molds were set as variables, the tensile strength, and Young's Modulus for five duplicates for each batch were set in analysis. The p-value was used to determine statistical significance, with differences considered significant if the p-value was below 0.05.

3 | RESULTS AND DISCUSSION

In this study, nine batches of specimens were fabricated using different techniques: FFF only, IM only, and overmolding with both metal and SLA-fabricated molds. A naming convention was established for clarity: M-IM indicates the full-size specimen injection molded using a metal mold, M-HTNJ refers to the overmolded specimen based on the half thickness with no joint configuration preform and S-HTMC means the overmolded specimen

—WILEY 5

FIGURE 3 CAD models of IM specimen and inserts utilized in overmolding stage: (A) full IM; (B) half thickness; (C) half thickness with male cube; (D) half thickness with female cube.[43]
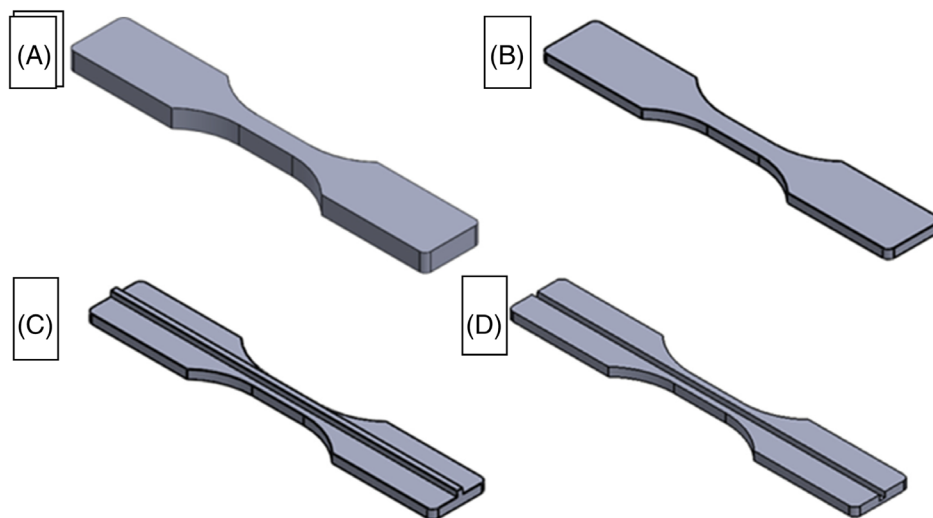
in the half thickness male cube configuration fabricated using an SLA mold.

3.1 | Manufacturing cost in molds and specimens

The manufacturing cost in mold fabrication can be normally divided into three parts: material, process, and energy.[44] In context of this, an introduction of SLA-fabricated mold represents a significant advancement due to their lower material and process cost and even design flexibility compared to traditional metal molds.[42] The production of two SLA-fabricated molds required only 12 h and approximately 30 euros for materials, a stark contrast to the several months and 5000 euros typically required for metal molds.

Furthermore, the ability to produce high-quality articles at minimal cost is a critical objective in the manufacturing industry.[45] In this study, fabricating a single FFF specimen required 12 min. In comparison, a full IM cycle producing two specimens took only 1.5 min. The overmolding technique, which combines the benefits of both FFF and IM, required 13.5 min to produce two finalized specimens, significantly reducing the manufacturing time compared to the FFF process alone. The majority of the time in the overmolding process was spent on insert fabrication (12 min), highlighting that overmolding effectively addresses the primary drawback of FFF—low manufacturing efficiency—by achieving a 40% reduction in fabrication time.

3.2 | Dimensional precision

The dimensions of all fabricated specimens, which were shown in Table 2, indicated that overmolded batches exhibited lower dimensional tolerance compared to FFF batches, consistent with previous findings.[12,36] Regarding to the difference between the SLA-fabricated batches and the metal mold batches, a tiny higher dimensional tolerance can be observed in the SLA batch. This phenomenon can be attributed to the following statements: 1. A greater stiffness, hardness, and resistance to deformation under pressure for the metal mold ensure a more stable shape and dimension throughout the IM process, especially under the high injection pressure and temperature; 2. The minor surface imperfections and layer lines due to the layer-by-layer fabrication manner in SLA can slightly affect the dimensional accuracy of finalized products; 3. The higher thermal conductivity of metal molds ensure an efficient and uniform cooling for the injection molded material, which reduces the warping, shrinkage, and other dimensional inaccuracies; 4. The less durable and more prone to wear after repeated process in SLA-fabricated mold can result in a gradual loss of dimensional precision over time.

3.3 | Tensile performance

The tensile performances of all fabricated specimens were evaluated based on maximum tensile strength (σ) and Young's Modulus (E), as displayed in Table 3. FFF batches demonstrated the lowest tensile performance (σ = 41.3 MPa, E = 823.1 MPa) compared to other batches (σ ranging from 46.9 to 61.7 MPa, E ranging from 883.2 to 983.5 MPa). This indicates a positive effect of the overmolding process on tensile performance. Low standard deviations in IM and overmolded batches suggest promising repeatability, which is beneficial for manufacturing consistency.[46]

In this study, the effects of different fabrication methods, mold types, and joint configurations on the

Parameter	FFF batch	Metal mold batch	SLA mold batch
Thickness	3.2 ± 0.2	3.2 ± 0.2	3.2 ± 0.2
Total length	64 ± 0.3	64 ± 0.1	64 ± 0.2
Width at two ends	10 ± 0.2	10 ± 0.1	10 ± 0.1

TABLE 2 Dimensions of all fabricated samples (all units are in mm).

TABLE 3 Tensile results of all fabricated specimens.

Batch	σ (MPa)	E (MPa)
FFF	41.3 ± 4.2	823.1 ± 18.6
M-IM	61.7 ± 0.9	963.2 ± 74.8
M-HTNJ	50.6 ± 2.1	959.3 ± 26.1
M-HTMC	54.5 ± 4.7	921.5 ± 34.7
M-HTFC	60.9 ± 0.5	969.0 ± 10.5
S-IM	55.9 ± 0.8	983.5 ± 72.9
S-HTNJ	46.9 ± 2.7	883.2 ± 53.6
S-HTMC	49.3 ± 2.7	956.8 ± 69.6
S-HTFC	51.5 ± 0.7	977.8 ± 66.4

FIGURE 4 Stress–strain curves for FFF and IM batches.

tensile performance of the finalized specimens are discussed in detail in the following sections. This discussion includes failure analysis based on stress–strain curves and SEM images, as well as statistical analysis using ANOVA.

3.3.1 | Effect of fabrication methods on tensile performance

As shown in Table 3, Figures 4, and 5, M-IM batches displayed the highest tensile strength ($\sigma = 61.7$ MPa) compared to M-overmolded batches ($\sigma = 50.6$–60.9 MPa) and FFF batch ($\sigma = 41.3$ MPa). Similarly, S-IM batches ($\sigma = 55.9$ MPa) outperformed other SLA-fabricated mold batches ($\sigma = 46.9$–51.5 MPa). The superior tensile performance of IM batches is attributed to better homogeneity, bonding, and fewer defects in IM processing,[47] reducing stress concentration and material weakness. The higher tensile performance of the IM batches compared to the overmolded batches can be explained by two main factors: (i) the interface between the substrate and the overmolded section may have defects and weak bonding, which reduce tensile strength; (ii) the varied cooling rates and thermal expansion between the inserts and the overmolded material can induce residual stresses, further reducing tensile strength. Despite the small difference in tensile strength between the IM and overmolded batches, the significant difference compared to the FFF batch indicates that overmolding is a highly recommended technique in the manufacturing industry. This technique not
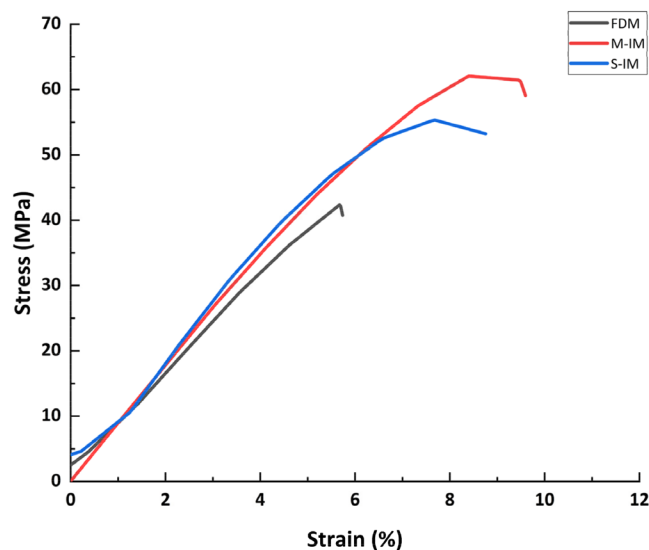
only provides promising mechanical properties but also allows for tailored characteristics, such as bespoke prostheses with enhanced bonding strength, fulfilling specific patient needs.

3.3.2 | Effect of joint configuration on tensile performance

The joint configurations achieved through the FFF machine offer high customization levels in overmolded articles. As presented in Table 3 and Figure 5, the female cube joint configuration (FC) resulted in the highest tensile strength (60.9 and 51.5 MPa) when using metal and SLA-fabricated molds, respectively. Additionally, the male cube joint configuration (MC) also showed superior tensile strength compared to the non-jointed (NJ) configurations (54.5 MPa for M-HTMC vs. 50.6 MPa for M-HTNJ and 49.3 MPa for S-HTMC vs. 46.9 MPa for S-HTNJ).

This finding is consistent with our previous studies on PLA material[2] and can be attributed to several factors: (i) the enhanced mechanical engagement due to the interlocking mechanism provided by the cube joint configuration, where protrusions and recesses fit together, enhances bonding strength by offering additional resistance to separation. In contrast, NJ configurations rely primarily on
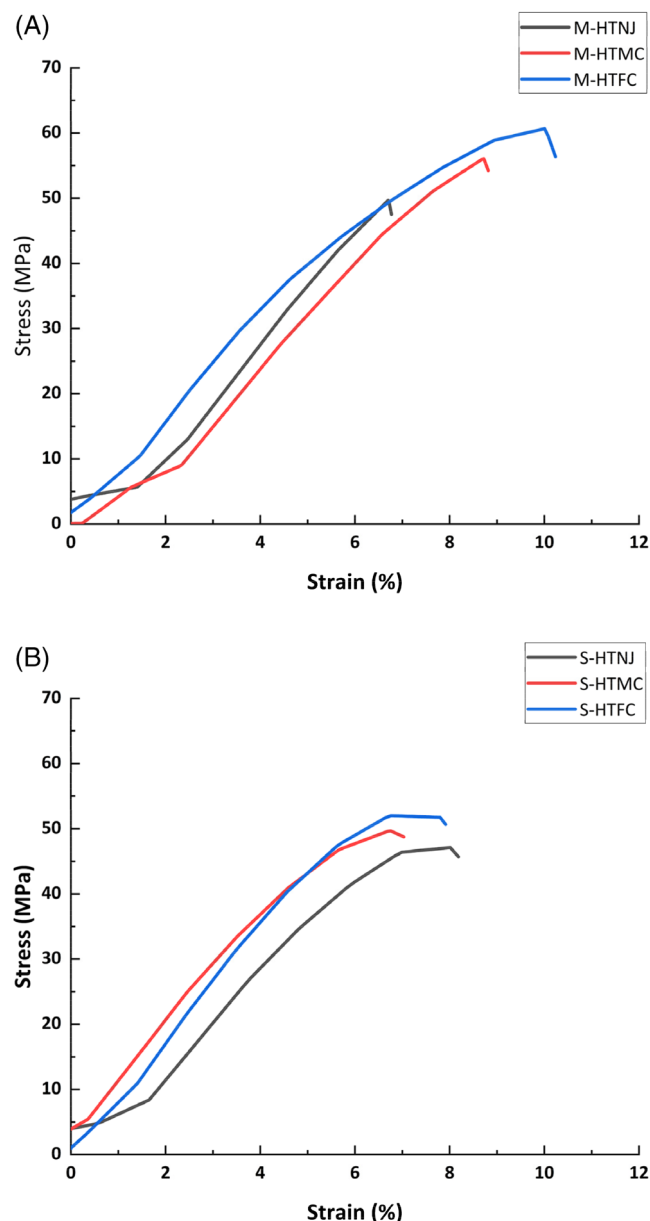
FIGURE 5 Stress–strain curves for all overmolded batches in function of employed molds: (A) metal mold and (B) SLA-fabricated mold.

adhesive or cohesive forces, which provide limited mechanical engagement; (ii) the increased contact area that the cube joint configuration offers a larger actual contact surface area between the two substrates compared to the NJ configuration. This larger contact area results in an enhanced grip and stronger overall bonding; and (iii) the improved stress distribution that the cube joint configuration as it distributes stress over multiple planes and directions, effectively bearing loads and reducing stress concentrations, thereby improving overall bonding strength. The results indicate that optimizing FFF parameters can significantly enhance the

quality of finalized articles. This optimization allows for personalization to meet customer demands and ensures robust and resilient bonds capable of withstanding greater forces and stresses without failure.

3.3.3 | Effect of mold type on tensile performance

The design and fabrication of molds pose significant challenges for IM users due to the need to balance manufacturing costs and production efficiency. To address this, an SLA technique was utilized to fabricate thermosetting resin molds for a comparative analysis with metal molds in producing overmolded specimens. As shown in Table 2 and Figure 5A for metal mold and (b) for SLA-fabricated mold, specimens fabricated using metal molds exhibited superior tensile performance (50.6–161.7 MPa) compared to those fabricated with SLA molds (46.9–55.9 MPa). This difference can be attributed to the properties of the mold materials and thermal management during the molding process. The superior thermal conductivity of metal molds facilitates uniform cooling and solidification of the material. This efficient thermal management prevents the accumulation of internal stresses and warping in the finalized specimens, thereby enhancing tensile performance. Moreover, the controlled cooling rate in metal molds is crucial for optimizing the molecular orientation of the polymer, resulting in higher quality samples.

3.4 | Morphological behavior

The SEM images of the cross sections of fractured tensile batches are displayed in Figure 6. A comparison between the batches fabricated using metal and SLA-fabricated molds reveals more ductile fracture behavior in the metal mold overmolding group (Figure 6D,F,H) compared to the predominantly brittle fracture behavior observed in the SLA-fabricated mold batches Figure 6C,E,G. This result aligns with the tensile results shown in Table 2 and Figure 5 and can be attributed to the lower thermal conductivity of thermosetting resin compared to metal. For example, overmolded specimens fabricated using SLA-fabricated molds experience uneven cooling rates at the interfaces where the majority of tensile loading is borne by the injection-molded materials. This results in residual stresses within the finalized specimen, leading to brittle behavior. Conversely, specimens produced using metal molds benefit from uniform cooling, reducing internal stresses, and enhancing ductility. Within the IM batches, a notable difference in ductility is observed between the SLA and metal mold specimens. Greater ductility is evident in Figure 6B
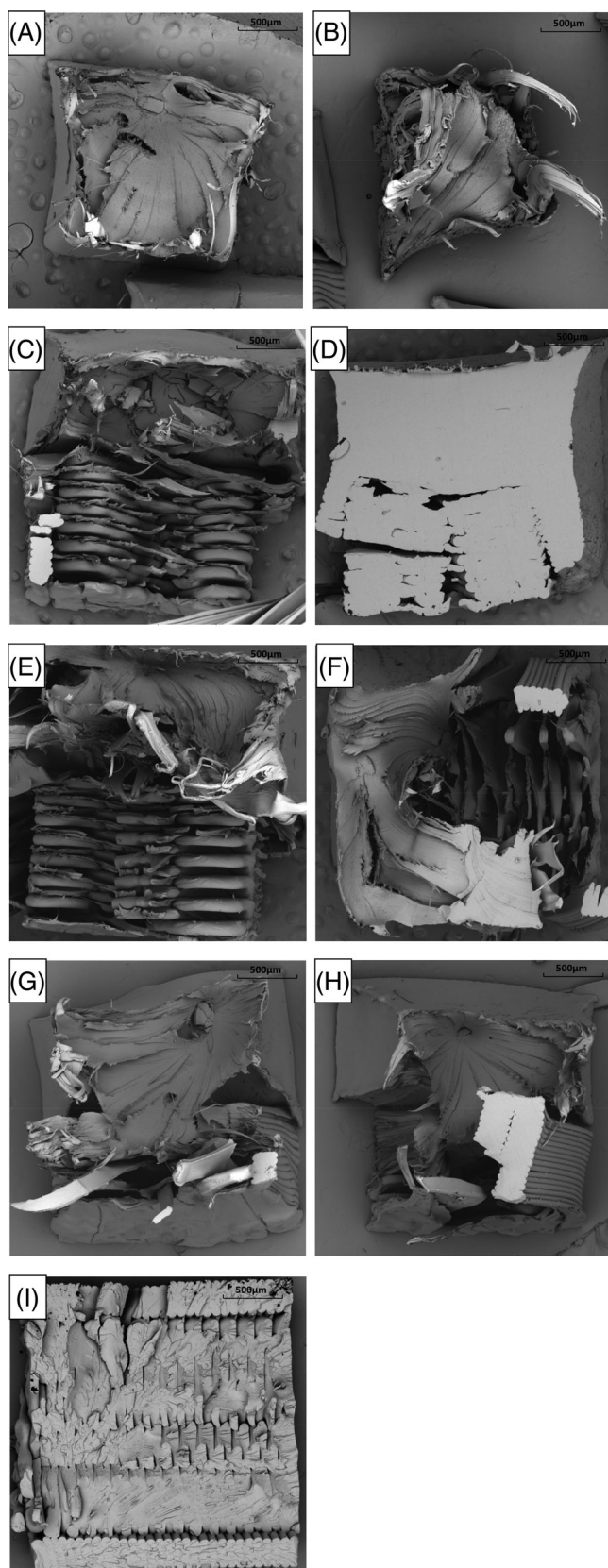
FIGURE 6 SEM images for the cross sections of failed tensile bars: (A) M-IM; (B) S-IM; (C) M-HT; (D) S-HT; (E) M-HTMC; (F) S-HTMC; (G) M-HTFC; (H) S-HTFC; and (I) FFF.

TABLE 4 ANOVA result of tensile strength, where the DF indicates the degree of freedom, SS indicates the standard deviation, and MS indicates the mean square.

Source	DF	SS	MS	*F*-Value	*p*-Value
JC	2	169.65	84.824	10.62	0.002
Mold	1	168.67	168.667	21.11	0
Error	14	111.85	7.99		
Lack-of-fit	2	27.43	13.717	1.95	0.185
Pure error	12	84.42	7.035		
Total	17	450.17			

compared to Figure 6A. This can be attributed to the low thermal conductivity of the SLA mold, which affects the polymer in a way that favors ductility.

Additionally, the FC batches exhibit more polymer entanglement compared to the NJ and MC batches, consistent with previous studies.[2,12,36] This increased entanglement contributes to improved mechanical properties. For the FFF batch (Figure 6I), a brittle tensile behavior can be observed, which is resulted from the weaker bonds between layers, voids in the internal structure, and internal stresses due to the less homogeneous structure and rapid cooling inherent to the FFF process.

3.5 | Statistical analysis

The ANOVA results shown in Table 4 indicate that both joint configuration and the mold type have a significant effect on tensile strength since the *p*-values of JC and mold are below 0.05 ($P_{JC} = 0.002$ and $P_{Mold} = 0$). Additionally, the higher *F*-value for the mold (21.11) compared to the joint configuration (10.62) demonstrates that the type of mold has a greater impact on tensile strength than the joint configuration (FFF inserts). This finding is consistent with the results discussed in Section 3.3.3, highlighting the critical role of mold material and design in determining the mechanical properties of the final specimens.

Regarding the Young's Modulus, the ANOVA results in Table 5 indicate that the joint configuration has a greater *F*-value (1.54) compared to the mold (0.19), suggesting a more pronounced impact from the joint configuration than from the type of mold. However, since their *p*-values are above 0.05, these effects are not statistically significant, indicating that neither the joint configuration nor the mold type has a significant influence on the Young's Modulus.

TABLE 5 ANOVA result of Young's Modulus, where the DF indicates the degree of freedom, SS indicates the standard deviation, and MS indicates the mean square.

Source	DF	SS	MS	*F*-Value	*p*-Value
JC	2	8437.7	4218.9	1.54	0.249
Mold	1	508.8	508.8	0.19	0.673
Error	14	38424.1	2744.6		
Lack-of-fit	2	10187.7	5093.9	2.16	0.157
Pure error	12	28236.4	2353		
Total	17	47370.6			

4 | CONCLUSION

This study used polyethylene terephthalate glycol (PETG) to proceed a comparative analysis in the tensile specimens fabricated using SLA-fabricated mold and metal mold, respectively.

The dimensions of all finalized specimens were first investigated and followed with the tensile performances. It can be seen that a higher dimension tolerance shown in the specimens manufactured by SLA-fabricated mold, which indicates a stable cavity geometry needs to be confirmed. In case of the tensile behaviors, consistent with our previous findings, the IM batch exhibited superior tensile behavior compared to the FFF and overmolding batches. Among the joint configurations, the FC joint configuration specimens demonstrated the highest tensile performance compared to the NJ and MC configurations. This can be attributed to enhanced mechanical engagement, greater contact area, and improved stress distribution in the FC batch.

Additionally, the tensile performance of SLA-fabricated mold batches was lower than that of metal mold batches, which can be attributed to the superior thermal conductivity of metal molds. This results in lower internal stresses and warping in the finalized specimens. Despite this, the ease of mold design and low fabrication cost of SLA-fabricated molds remain significant advantages over metal molds. This suggests a promising future for SLA-fabricated molds in the overmolding process, particularly for applications requiring bespoke characteristics, such as home appliances. Future work will focus on exploring methods to enhance the service life and broaden the application scope of SLA-fabricated molds concerning the overmolding technique.

AUTHOR CONTRIBUTIONS

All authors contributed to the study conception and design. Material preparation was performed by Xun Jian, Ke Gong, Yinshi Lu, Vicente Moritz, Alexandre Portela, and Ian Major; data collection was performed by Ke Gong, Yinshi Lu and Alexandre Portela; analysis was performed by Xun Jian, Ke Gong, and Wenyi Du. The first draft of the manuscript was written by Xun Jian, Ke Gong, and Ian Major. The manuscript was finalized by Ke Gong, Vicente Moritz, Alexandre Portela, and Ian Major. All authors read and approved the final manuscript.

CONFLICT OF INTEREST STATEMENT
The authors declare no competing interests.

DATA AVAILABILITY STATEMENT
The data that support the findings of this study are available from the corresponding author, IM, upon reasonable request.

ORCID
Ke Gong https://orcid.org/0000-0003-1144-8292
Vicente Moritz https://orcid.org/0000-0001-9146-5492
Alexandre Portela https://orcid.org/0009-0001-6137-9507
Ian Major https://orcid.org/0000-0002-0538-9786

REFERENCES
1. Szuchács A, Ageyeva T, Boros R, Kovács JG. Bonding strength calculation in multicomponent plastic processing technologies. *Mater Manuf Process.* 2022;37(2):151-159. doi:10.1080/10426914.2021.1948052
2. Gong K, Liu H, Huang C, et al. Mass customization of polylactic acid (PLA) parts via a hybrid manufacturing process. *Polymers (Basel).* 2022;14(24):5413. doi:10.3390/polym14245413
3. Ryan LE. *Utilization of Lattice Structures for Increased Interface Strength in Overmolded Silicone and Additively Manufactured Parts.* Master, Pennsylvania State University; 2020.
4. Nguyen S, Perez CJ, Desimone M, Pastor JM, Tomba JP, Carella JM. Adhesion control for injection overmolding of elastomeric propylene copolymers on polypropylene. Effects of block and random microstructures. *Int J Adhes Adhes.* 2013;46:44-55. doi:10.1016/j.ijadhadh.2013.05.016
5. Aliyeva N, Sas HS, Saner Okan B. *Recent Developments on the Overmolding Process for the Fabrication of Thermoset and Thermoplastic Composites by the Integration of Nano/Micron-Scale Reinforcements.* Elsevier Ltd; 2021. doi:10.1016/j.compositesa.2021.106525
6. Yu L, Xia B, Zhang J, Peng B. Effect of temperature related processing parameters on the interface bonding strength of automotive overmolding injection parts. *Mater Test.* 2019;61(10):960-964. doi:10.3139/120.111408

7. Novák M, Rosina J, Bendová H, et al. Low-cost and prototype-friendly method for biocompatible encapsulation of implantable electronics with epoxy overmolding, hermetic feedthroughs and P3HT coating. *Sci Rep*. 2023;13(1):1644. doi:10.1038/s41598-023-28699-6

8. Boros R, Tatyana A, Golcs Á, Krafcsik OH, Kovács JG. Plasma treatment to improve the adhesion between ABS and PA6 in hybrid structures produced by injection overmolding. *Polym Test*. 2022;106:107446. doi:10.1016/j.polymertesting.2021.107446

9. Boros R, Rajamani PK, Kovács JG. Thermoplastic overmolding onto injection-molded and in situ polymerization-based polyamides. *Materials*. 2018;11(11):2140. doi:10.3390/ma11112140

10. Ogle RC. *Optimized 3D-Printing of Carbon Fiber-Reinforced Polyether-Ether-Ketone (CFR-PEEK) for Use in Overmolded Lattice Composite*. Master, University of Tennessee; 2022 [Online]. Available at: https://trace.tennessee.edu/utk_gradthes/7066

11. Boros R, Kannan Rajamani P, Kovács JG. Combination of 3D printing and injection molding: overmolding and overprinting. *Express Polym Lett*. 2019;13(10):889-897. doi:10.3144/expresspolymlett.2019.77

12. Gong K, Liu H, Huang C, Cao Z, Fuenmayor E, Major I. Hybrid manufacturing of acrylonitrile butadiene styrene (ABS) via the combination of material extrusion additive manufacturing and injection molding. *Polymers (Basel)*. 2022;14:5093.

13. Sang L, Han S, Li Z, Yang X, Hou W. Development of short basalt fiber reinforced polylactide composites and their feasible evaluation for 3D printing applications. *Compos B Eng*. 2019;164:629-639. doi:10.1016/j.compositesb.2019.01.085

14. Goyanes A, Scarpa M, Kamlow M-A, Gaisford S, Basit A, Orlu M. Patient acceptability of 3D printed medicines. *Int J Pharm*. 2017;530:71-78. doi:10.1016/j.ijpharm.2017.07.064

15. Li Z, Li Y, Wang G. Flexural properties and fracture behavior of CF/PEEK in orthogonal building orientation by FDM: microstructure and mechanism. *Polymers (Basel)*. 2019;11(4):656. doi:10.3390/polym11040656

16. Silva M, Felismina R, Mateus A, Parreira P, Malça C. Application of a hybrid additive manufacturing methodology to produce a metal/polymer customized dental implant. *Procedia Manuf*. 2017;12:150-155. doi:10.1016/j.promfg.2017.08.019

17. Liu Y, Liang X, Saeed A, Lan W, Qin W. Properties of 3D printed dough and optimization of printing parameters. *Innov Food Sci Emerg Technol*. 2019;54(February):9-18. doi:10.1016/j.ifset.2019.03.008

18. Hanemann T, Klein A, Baumgärtner S, Jung J, Wilhelm D, Antusch S. Material extrusion 3D printing of PEEK-based composites. *Polymers (Basel)*. 2023;15(16):3412. doi:10.3390/polym15163412

19. Andreu A, Kim S, Dittus J, Friedmann M, Fleischer J, Yoon YJ. Hybrid material extrusion 3D printing to strengthen interlayer adhesion through hot rolling. *Addit Manuf*. 2022;55:102773. doi:10.1016/j.addma.2022.102773

20. Giorleo L, Stampone B, Trotta G. Micro injection moulding process with high-temperature resistance resin insert produced with material jetting technology: effect of part orientation. *Addit Manuf*. 2022;56:102947. doi:10.1016/j.addma.2022.102947

21. Joo H, Cho S. Comparative studies on polyurethane composites filled with polyaniline and graphene for DLP-type 3D printing. *Polymers (Basel)*. 2020;12(1):67. doi:10.3390/polym12010067

22. Van Der Walt S, Du Preez S, Du Plessis JL. Particle emissions and respiratory exposure to hazardous chemical substances associated with binder jetting additive manufacturing utilizing poly methyl methacrylate. *Hyg Environ Health Adv*. 2022;4:100033. doi:10.1016/j.heha.2022.100033

23. Englert L, Heuer A, Engelskirchen MK, et al. Hybrid material additive manufacturing: interlocking interfaces for fused filament fabrication on laser powder bed fusion substrates. *Virtual Phys Prototyp*. 2022;17(3):508-527. doi:10.1080/17452759.2022.2048228

24. Bai S, Wei L, He C, et al. Effects of layer thickness ratio on the bendability of Mg-Al-Zn/Mg-Gd laminated composite sheet. *J Mater Res Technol*. 2022;21:1013-1028. doi:10.1016/j.jmrt.2022.09.101

25. Kurfess R, Kannan R, Feldhausen T, Saleeby K, Hart AJ, Hardt D. Towards directed energy deposition of metals using polymer-based supports: hardness of 316L stainless steel deposited on carbon-fiber-reinforced ABS. *Volume 2: Manufacturing Processes; Manufacturing Systems*. American Society of Mechanical Engineers; 2022. doi:10.1115/MSEC2022-85562

26. Zhao Y, Chen Y, Zhou Y. Novel mechanical models of tensile strength and elastic property of FDM AM PLA materials: experimental and theoretical analyses. *Mater Des*. 2019;181:108089. doi:10.1016/j.matdes.2019.108089

27. Hu G, Cao Z, Hopkins M, et al. Optimizing the hardness of SLA printed objects by using the neural network and genetic algorithm. *Procedia Manufacturing*. Vol 38. Elsevier B.V; 2019:117-124. doi:10.1016/j.promfg.2020.01.016

28. Palmić TB, Slavič J, Boltežar M. Process parameters for FFF 3D-printed conductors for applications in sensors. *Sensors (Switzerland)*. 2020;20(16):1-21. doi:10.3390/s20164542

29. Crump S. Apparatus and method for creating three-dimensional objects. Available at: https://patents.google.com/patent/US5121329A/en, United States Patent 19, p. 15 1992. doi:10.2116/bunsekikagaku.28.3_195

30. Yavas D. High-temperature fracture behavior of carbon fiber reinforced PEEK composites fabricated via fused filament fabrication. *Compos B Eng*. 2023;266:110987. doi:10.1016/j.compositesb.2023.110987

31. Birosz MT, Ledenyák D, Andó M. Effect of FDM infill patterns on mechanical properties. *Polym Test*. 2022;113:107654. doi:10.1016/j.polymertesting.2022.107654

32. Dawoud M, Taha I, Ebeid SJ. Mechanical behaviour of ABS: an experimental study using FDM and injection moulding techniques. *J Manuf Process*. 2016;21:39-45. doi:10.1016/j.jmapro.2015.11.002

33. He Y, Shen M, Wang Q, Wang T, Pei X. Effects of FDM parameters and annealing on the mechanical and tribological properties of PEEK. *Compos Struct*. 2023;313:116901. doi:10.1016/j.compstruct.2023.116901

34. Haryńska A, Gubanska I, Kucinska-Lipka J, Janik H. Fabrication and characterization of flexible medical-grade TPU filament for fused deposition modeling 3DP technology. *Polymers (Basel)*. 2018;10(12):1304. doi:10.3390/polym10121304

35. Fuenmayor E, O'Donnell C, Gately N, et al. Mass-customization of oral tablets via the combination of 3D printing and injection molding. *Int J Pharm*. 2019;569(July):118611. doi:10.1016/j.ijpharm.2019.118611

36. Gong K, Xu H, Liu H, Cao Z, Fuenmayor E, Major I. Hybrid manufacturing of mixed-material bilayer parts via injection

molding and material extrusion three-dimensional printing. *J Appl Polym Sci.* 2023;140:e53972. doi:10.1002/app.53972

37. Rajamani PK, Ageyeva T, Kovács JG. Personalized mass production by hybridization of additive manufacturing and injection molding. *Polymers (Basel).* 2021;13(2):1-19. doi:10.3390/polym13020309

38. Smith JA, Basgul C, Mohammadlou BS, Allen M, Kurtz SM. Investigating the feasibility and performance of hybrid over-molded UHMWPE 3D-printed PEEK structural composites for orthopedic implant applications: a pilot study. *Bioengineering.* 2024;11(6):616. doi:10.3390/bioengineering11060616

39. Hu G, Cao Z, Hopkins M, Lyons JG, Brennan-Fournet M, Devine DM. Nanofillers can be used to enhance the thermal conductivity of commercially available SLA resins. *Procedia Manufacturing.* Vol 38. Elsevier B.V; 2019:1236-1243. doi:10.1016/j.promfg.2020.01.215

40. Moritz VF, Bezerra GSN, Hopkins Jnr M, et al. Heat dissipation plays critical role for longevity of polymer-based 3D-printed inserts for plastics injection moulding. *J Manuf Mater Process.* 2022;6(5):117. doi:10.3390/jmmp6050117

41. Basile V, Modica F, Surace R, Fassi I. Micro-texturing of molds via Stereolithography for the fabrication of medical components. *Procedia CIRP.* Vol 110. Elsevier B.V; 2022:93-98. doi:10.1016/j.procir.2022.06.019

42. Keane G, Healy AV, Devine DM. Post-process considerations for photopolymer 3D-printed injection moulded insert tooling applications. *J Compos Sci.* 2024;8(4):151. doi:10.3390/jcs8040151

43. Gong K. *Integrating 3D Printing and Injection Molding for Mass Customization: Advancements in Hybrid Manufacturing.* PhD, Technological University of Shannon, Athlone; 2023.

44. Folgado R, Peças P, Henriques E. Life cycle cost for technology selection: a case study in the manufacturing of injection moulds. *Int J Prod Econ.* 2010;128:368-378. doi:10.1016/j.ijpe.2010.07.036

45. Gong K, Liu H, Xu H, et al. Optimizing process parameters of a material extrusion-based overprinting technique for the fabrication of tensile specimens. *Int J Adv Manuf Technol.* 2023;127(7–8):3513-3524. doi:10.1007/s00170-023-11720-7

46. Zhai W, Wang P, Ng FL, Zhou W, Nai SML, Wei J. Hybrid manufacturing of γ-TiAl and Ti–6Al–4V bimetal component with enhanced strength using electron beam melting. *Compos B Eng.* 2021;207:108587. doi:10.1016/j.compositesb.2020.108587

47. Lay M, Thajudin NLN, Hamid ZAA, Rusli A, Abdullah MK, Shuib RK. Comparison of physical and mechanical properties of PLA, ABS and nylon 6 fabricated using fused deposition modeling and injection molding. *Compos B Eng.* 2019;176:107341. doi:10.1016/j.compositesb.2019.107341